

Optical pumping of Cs atoms in solid ^4He

S. Lang,^{1,2} S. Kanorsky,^{1,3} T. Eichler,¹ R. Müller-Siebert,¹ T. W. Hänsch,² and A. Weis^{1,2}

¹*Institut für Angewandte Physik, Universität Bonn, Wegelerstrasse 8, D-53115 Bonn, Germany*

²*Max-Planck-Institut für Quantenoptik, Hans-Kopfermann-Strasse 1, D-85748 Garching, Germany*

³*Lebedev Physical Institute, Leninsky Prospekt 53, 117924 Moscow, Russia*

(Received 20 May 1999)

We have studied both theoretically and experimentally the optical pumping of Cs atoms trapped in (body-centered-cubic and hexagonal-close-packed) crystalline ^4He matrices. The theoretical approach is based on rate equations for which time-dependent and asymptotic solutions are obtained in the case of depopulation and repopulation pumping. Comparison with experiments show that repopulation pumping, i.e., a process in which spin polarization in the excited state is not destroyed, is the dominant pumping mechanism in both crystalline phases. [S1050-2947(99)07410-7]

PACS number(s): 32.30.Dx, 32.10.Fn, 76.70.Hb, 67.80.Mg

I. INTRODUCTION

Spectroscopic studies of atoms isolated in rare-gas matrices of Ne, Ar, Kr, and Xe have been performed for more than 40 years. The study of the magnetic properties of matrix isolated metal atoms by conventional low temperature electron-spin resonance and nuclear magnetic resonance spectroscopy in high magnetic fields [1] has played an important role in these investigations. In 1994 the rare-gas matrix isolation technique was extended to solid helium matrices [2] by applying an implantation technique first demonstrated for the immersion of foreign atoms into superfluid helium [3,4]. The first observation of low-field magnetic resonance transitions of Cs and Rb in *superfluid* helium was reported in 1994 [5,6], and in 1995 magnetic resonance of Cs atoms in *solid* helium was observed [7]. The powerful technique of optical pumping by polarized resonance radiation was used in these experiments to create a very high degree of both electronic and nuclear-spin polarization. To our knowledge the latter experiment represents the first demonstration of optically created atomic spin polarization in any solid rare-gas matrix. The polarization technique together with the highly efficient detection of magnetic resonance via the monitoring of atomic fluorescence (or absorption) has opened the new field of optically detected magnetic resonance (ODMR) spectroscopy of paramagnetic impurities in solid helium. Extremely long longitudinal and transverse electronic spin relaxation times were observed in Cs atoms trapped in the cubic phase of solid ^4He [7,8]. Atomic impurities in condensed helium are a new spectroscopic tool for the study of quantum liquids and solids, and offer a promising approach for the study of fundamental physics, such as the search for permanent electric dipole moments of atoms [9]. The properties of atomic and molecular defects in condensed helium were recently reviewed by several authors [10–12].

Helium is the lightest rare-gas atom, and has the smallest electric polarizability. The zero-point kinetic energy of condensed He is comparable with the interatomic potential energy and the strong delocalization due to the large amplitude of the zero-point vibrations leads to a strong overlap of the wave functions of adjacent atoms. The large kinetic energy

associated with the zero-point motion of the helium atoms forces the molar volume of condensed He to be much larger than expected from the interatomic potentials only. As a consequence condensed helium forms a quantum liquid (crystal) which is extremely compressible. A pressure of more than 25 bar is needed in order to solidify He even at $T=0$ K. The softness of solid helium is also responsible for another important property which distinguishes it from any other solid-state matrix. The Pauli exchange interaction of an implanted one-electron impurity atom with the surrounding closed-shell helium atoms repels the latter and leads to the formation of a defect structure which is commonly called an “atomic bubble.” The shape of this bubble is mainly determined by the symmetry of the wave function of the implanted atom, although slight deviations from this simplified view were recently reported [13]. The interaction of implanted atoms with the He matrix strongly perturbs the optical transition frequencies [10]. Line shifts of the absorption lines of several 10 nm, and a broadening by several nm are typical for the D_1 transitions in heavy alkali metals, whereas the emission lines are in general less broadened and less shifted.

In contrast to the heavier noble gas matrices, which solidify in a face-centered-cubic (fcc) structure, helium can crystallize (at pressures below 1000 bar) in either a hexagonal close-packed (hcp) phase or a body-centered-cubic (bcc) phase. ^4He has neither a nuclear nor an electronic magnetic moment. This property, together with the high degree of spherical symmetry of the atomic bubbles, makes solid helium an ideal host matrix for the study of the magnetic properties of imbedded paramagnetic atoms as long spin relaxation and dephasing times and hence very narrow magnetic resonance lines can be observed. In this paper we focus on the optical pumping process of Cs atoms implanted in either bcc or hcp He matrices. We derive the optical pumping equations for this particular sample for the two extreme situations of repopulation and depopulation pumping, and show, by comparison with experiment, that in both phases the pumping is dominated by repopulation.

II. THEORY

It has been since the early 1950s that the irradiation of paramagnetic atoms with circularly polarized resonance ra-

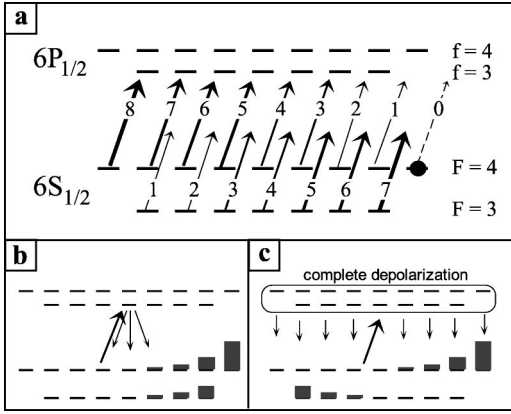


FIG. 1. (a) Hyperfine Zeeman levels of the Cs D_1 line. The numbered arrows indicate the relative line strengths of the transitions involved in the optical pumping process under irradiation with σ_+ light. The $F=4, M=4$ (dark) state does not couple to the light field. (b) Relative populations (indicated by bar heights) of the hyperfine ground states under repopulation (Kastler-type) pumping. (c) Relative steady-state populations of the hyperfine ground states under depopulation (Dehmelt-type) pumping).

diation can produce a very high degree of electronic spin polarization in the atomic ground state [14]. This process is known as optical pumping. In this section we first apply the theory of optical pumping to describe the evolution of the magnetic sublevel populations of the $6S_{1/2}$ ground state of Cs atoms implanted in crystalline helium matrices when the sample is excited with circularly polarized light tuned to the D_1 ($6^2S_{1/2}-6^2P_{1/2}$) transition. The relevant hyperfine structure of this transition is shown in Fig. 1. We then discuss how the spin-polarized sample affects the scattering rate (fluorescence yield) of optical resonance radiation, and how it can be used to monitor the depolarization induced by magnetic resonance transitions efficiently in the atomic ground state.

The interaction of the implanted Cs atoms with the He matrix causes the Cs D_1 -absorption line to be shifted from 894 nm in vacuum to 850 nm in solid ^4He with a homogeneous optical linewidth of ≈ 10 nm [2]. The hyperfine splittings in neither the excited nor ground state (1.2 and 9.2 GHz, respectively) can be resolved in the optical spectra. The steady-state distribution of the ground-state populations depends critically on the nature of the optical pumping process, i.e., on the interaction of the transient magnetization in the excited state with the helium matrix. In the following we will treat two extreme situations. When the polarization in the excited $6P_{1/2}$ state is totally destroyed by the interaction with the He matrix, the optical pumping process is referred to as “depopulation” or Dehmelt-type pumping [15]. On the other hand, one speaks of “repopulation” or Kastler-type pumping [15] when the polarization in the excited state is totally preserved during the optical-absorption-emission cycle.

We will use the following notation for the different hyperfine Zeeman sublevels in the basis of the total angular momentum eigenstates:

$$|F, M\rangle := |6S_{1/2}, I=7/2, F, M\rangle,$$

$$|f, m\rangle := |6P_{1/2}, I=7/2, f, m\rangle.$$

When the atoms are irradiated with circularly polarized (σ_+) light all Zeeman levels in the ground state are depopulated by absorption, except for the $|F=4, M=4\rangle$ state, which does not couple to σ_+ circularly polarized light and which we therefore refer to as a “dark state.” Spontaneous emission, on the other hand, populates all ground-state sublevels. Under continuous optical excitation the population in the $|4, +4\rangle$ state will therefore increase steadily, and the sample becomes more and more transparent with a corresponding decrease of the fluorescence intensity. As circularly polarized light couples only to level populations the knowledge of sublevel coherences is irrelevant for the understanding of the optical pumping process, and the theoretical description reduces to finding the solutions of a system of incoherent rate equations.

A. Optical pumping equations

The rate equations describing the evolution of the populations $p_{F,M}$ of the 16 sublevels $|F, M\rangle$ of the ground state and the 16 sublevels $|f, m\rangle$ of the excited state under the influence of a circularly (σ_+) polarized optical pumping field are given by

$$\begin{aligned} \dot{p}_{F,M} = & -\Gamma_p^{F,M,f,m} p_{F,M} + \sum_{f,m} \Gamma_{\text{spont}}^{f,m,F,M} p_{f,m} \\ & - \gamma_1 (p_{F,M} - p_{F,M}^{(0)}), \end{aligned} \quad (2.1)$$

$$\dot{p}_{f,m} = + \sum_{F,M} \Gamma_p^{F,M,f,m} p_{F,M} - \Gamma_{\text{spont}}^{\text{tot}} p_{f,m}. \quad (2.2)$$

$\Gamma_p^{F,M,f,m}$ is the optical pumping rate of the $|F, M\rangle \rightarrow |f, m = M+1\rangle$ transition, $\Gamma_{\text{spont}}^{f,m,F,M}$ is the spontaneous emission rate from the excited state $|f, m\rangle$ toward the state $|F, M\rangle$, and $\Gamma_{\text{spont}}^{\text{tot}} = \sum_{F', M'} \Gamma_{\text{spont}}^{f,m,F', M'}$ is the total spontaneous emission rate. The quantities $p_{F,M}^{(0)}$ are the ground-state populations in thermal equilibrium, and γ_1 is the relaxation rate of the ground-state populations which we assume to be isotropic, i.e., independent of F and M . The rate $\Gamma_{\text{spont}}^{\text{tot}} \approx 10^8 \text{ s}^{-1}$ at which the populations in the excited $6P_{1/2}$ state evolve exceeds the depopulation rate $\Gamma_p \approx 10^3 \text{ s}^{-1}$ of the ground-state populations by five orders of magnitude. On the time scale of the ground-state evolution, we can neglect the very fast transient processes in the excited state by setting $\dot{p}_{f,m} = 0$. The excited-state level populations—assumed to be negligible on average (no saturation of the optical transition)—can thus be eliminated, and the rate equations (2.2) are simplified to a system which involves ground-state populations only:

$$\begin{aligned} \dot{p}_{F,M} = & -\Gamma_p^{F,M,f,m} p_{F,M} \\ & + \sum_{\substack{F', M' \\ f, m}} \Gamma_{\text{spont}}^{f,m,F,M} \Gamma_p^{F', M', f, m} p_{F', M'} \frac{1}{\Gamma_{\text{spont}}^{\text{tot}}} \\ & - \gamma_1 (p_{F,M} - p_{F,M}^{(0)}). \end{aligned} \quad (2.3)$$

The three terms on the right side in Eq. (2.3) represent depopulation, repopulation, and relaxation processes of the ground-state levels.

The depopulation of the atomic ground states is due to the interaction with the optical pumping light, which we describe as a plane wave $E_q(z,t) = E e_q \cos(\omega t - kz)$ with amplitude E and polarization component e_q , where $q=0$ and ± 1 represent π - and σ_{\pm} -polarized light. The depopulation rate is given by

$$\Gamma_p(F, M, f, m) = \frac{\Omega^2}{\gamma_{\text{hom}}} = \frac{1}{\gamma_{\text{hom}}} \frac{E^2}{\hbar^2} |\langle f, m | d_q | F, M \rangle|^2,$$

where γ_{hom} is the homogeneous optical linewidth, and Ω is the Rabi frequency of the $FM \leftrightarrow fm$ transition.

Repopulation of the ground states is due to spontaneous emission only. While the Cs atoms are in the excited $6P_{1/2}$ state the shape of the He bubble relaxes with the Debye frequency ($\approx 10^{12} \text{ s}^{-1}$) of solid helium, which is nine orders of magnitude larger than the optical pumping rate (typically 10^3 s^{-1}). As the transition wavelength depends on the size and shape of the bubble, the exciting light can no longer deexcite the $6P_{1/2}$ state in the relaxed bubble, and stimulated emission can therefore be neglected.

The second term in Eq. (2.1) describes spontaneous emission

$$\sum_{f,m} \Gamma_{\text{spont}}^{f,m,F,M} p_{f,m} = \sum_{F',M'} p_{F',M'} \Gamma_p^{F',M',f,m} \frac{\Gamma_{\text{spont}}^{f,m,F,M}}{\Gamma_{\text{spont}}^{\text{tot}}}, \quad (2.4)$$

with the spontaneous emission rate

$$\Gamma_{\text{spont}}^{f,m,F,M} \propto \sum_q |\langle f, m | d_q | F, M \rangle|^2. \quad (2.5)$$

The total spontaneous emission rate $\Gamma_{\text{spont}}^{\text{tot}}$ is the sum of the decay rates from a given excited state $|f, m\rangle$ into all possible ground states $|F', M'\rangle$. Using orthogonality relations of the $3j$ and $6j$ symbols, the sum over F' and M' can be reduced to

$$\Gamma_{\text{spont}}^{\text{tot}} \propto \frac{1}{2j+1} |\langle j || d || J \rangle|^2. \quad (2.6)$$

With Eqs. (2.6) and (2.5), for the repopulation rate of the ground state $|F, M\rangle$ one deduces from Eq. (2.4),

$$\begin{aligned} \Gamma_{\text{repop}} &\equiv \sum_{f,m} \Gamma_{\text{spont}}^{f,m,F,M} p_{f,m} = \sum_{F',M'} p_{F',M'} \Gamma_p^{F',M',f,m} \\ &\times (2j+1) \frac{|\langle f, m | d_{M-m} | F, M \rangle|^2}{|\langle j || d || J \rangle|^2}. \end{aligned} \quad (2.7)$$

This equation describes the transfer of populations by fluorescence under *repopulation* pumping for which the polarization of the excited state is preserved.

In the case of *depopulation* pumping, in which the polarization in the excited state is completely destroyed, each

ground state $|F, M\rangle$ will be repopulated by spontaneous emission with equal probability. Taking the 16-fold degeneracy of the ground state into account, the depopulation rate is given by

$$\Gamma_{\text{depop}} \equiv \sum_{f,m} \Gamma_{\text{spont}}^{f,m,F,M} p_{f,m} = \sum_{F',M'} p_{F',M'} \Gamma_p^{F',M',f,m} \frac{1}{16}. \quad (2.8)$$

Note that Γ_{repop} depends on F and M , while Γ_{depop} is independent of F and M .

The third term in Eq. (2.1) describes relaxation in the ground state. The steady-state populations $p_{F,M}^{(0)}$ in the hyperfine states $F=4$ and 3 are determined by the Boltzmann factor. For a normalized total ground-state population ($\sum_{F,M} p_{F,M}^{(0)} = 1$) the thermal populations are given by

$$p_{F=3,M}^{(0)} = \frac{1}{7+9 \exp\left(-\frac{h\nu_{\text{hfs}}}{kT}\right)}, \quad (2.9)$$

$$p_{F=4,M}^{(0)} = \frac{1}{9+7 \exp\left(\frac{h\nu_{\text{hfs}}}{kT}\right)}, \quad (2.10)$$

where the hyperfine splitting ν_{hfs} is 9.2 GHz. In thermal equilibrium at 1.6 K, 51 % of all Cs atoms are in the $F=3$ state. In the experiments the thermal population distribution of the sublevels within each hyperfine ground state can be neglected. As a result we obtain the following set of differential equations governing the populations in the Cs ground states $|F, M\rangle$ for optical pumping with light of polarization e_q .

For optical repopulation pumping,

$$\begin{aligned} \dot{p}_{F,M} &= -\gamma_p \sum_f \mathcal{R}_{F,M,f,M+q} p_{F,M} + \gamma_p (2j+1) \\ &\times \sum_{F',M'} p_{F',M'} \mathcal{R}_{F',M',f,M'+q} \mathcal{R}_{f,M'+q,F,M} \\ &- \gamma_1 (p_{F,M} - p_{F,M}^{(0)}), \end{aligned} \quad (2.11)$$

and for optical depopulation pumping,

$$\begin{aligned} \dot{p}_{F,M} &= -\gamma_p \sum_f \mathcal{R}_{F,M,f,M+q} p_{F,M} \\ &+ \gamma_p \frac{1}{16} \sum_{F',M'} \mathcal{R}_{F',M',f,M'+q} p_{F',M'} \\ &- \gamma_1 (p_{F,M} - p_{F,M}^{(0)}), \end{aligned} \quad (2.12)$$

where

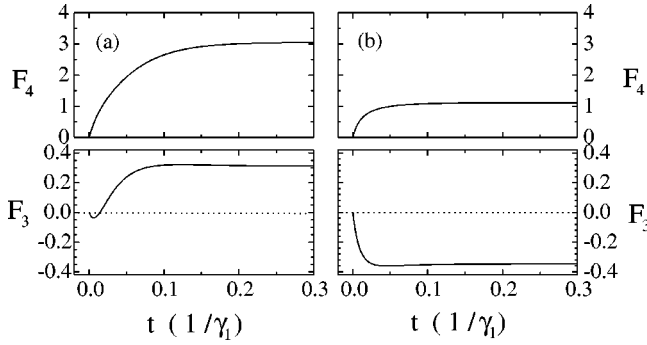


FIG. 2. Calculated time evolution of the buildup of hyperfine polarizations $F_3 = \langle F_z \rangle_3$ and $F_4 = \langle F_z \rangle_4$ under repopulation pumping (a) and depopulation pumping (b). The degree of circular polarization of the pump beam ξ_{pol} was chosen to be 80%, and the normalized pump rate γ_p/γ_1 was set to 700.

$$\mathcal{R}_{F,M,f,m} = (2F+1)(2f+1) \times \begin{pmatrix} f & 1 & F \\ -m & m-M & M \end{pmatrix}^2 \begin{Bmatrix} j & f & I \\ F & J & 1 \end{Bmatrix}^2. \quad (2.13)$$

The optical pumping rate γ_p is given by

$$\gamma_p = \frac{1}{\gamma_{\text{hom}}} \frac{E^2}{\hbar^2} | \langle j || d || J \rangle |^2. \quad (2.14)$$

In the experiments the light beam has to propagate through a number of cold windows, some of which are under pressure and have a pronounced stress-induced birefringence. Although we try to compensate for such effects by a careful adjustment of the polarization of the beam entering the cryostat, the polarization of the light reaching the sample is usually significantly less than 100%. Moreover, the hcp phase of helium is birefringent, and polycrystalline hcp samples depolarize the light beam further. In order to account for this effect we introduce a parameter ξ_{pol} , which describes the degree of circular polarization of the pumping light. ξ_{pol} is equal to ± 1 for 100% of σ_{\pm} polarization. In the numerical calculations discussed below the ground-state populations are first determined for σ_+ and for σ_- -polarized light.¹ The (incoherently) averaged value of $p_{F,M}$ is then given by

$$p_{F,M} = \frac{1 + \xi_{\text{pol}}}{2} p_{F,M}(\sigma_+) + \frac{1 - \xi_{\text{pol}}}{2} p_{F,M}(\sigma_-). \quad (2.15)$$

Note that one can show, by a calculation similar to the one presented in the Appendix, that in the case of unresolved hyperfine structure (present here) linearly polarized light will not redistribute sublevel populations. For this reason the linearly polarized content of an elliptically polarized beam will not contribute to the optical pumping process and can therefore be ignored. The physics of this property can be under-

¹In practice the calculation is performed for σ_+ light only, and the populations $p_{F,M}(\sigma_-)$ are obtained by using $p_{F,M}(\sigma_-) = p_{F,-M}(\sigma_+)$.

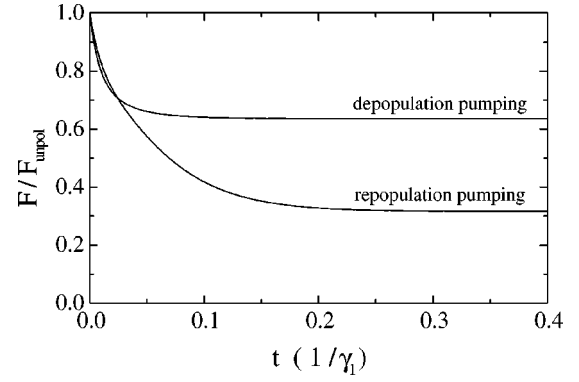


FIG. 3. Calculated time evolution of the normalized fluorescence signal $\mathcal{F}/\mathcal{F}_{\text{unpol}} = 1 - 2\langle J_z \rangle$. The parameters ξ_{pol} and γ_p/γ_1 are the same as in Fig. 2.

stood on the basis of a symmetry argument. The hyperfine structure of the coupled levels $6S_{1/2}$ and $6P_{1/2}$ is not resolved in the optical spectrum, and the pumping process thus involves only spherical symmetric states, whose rotational symmetry cannot be broken by the interaction with linearly polarized light. Optical pumping will therefore not affect the level populations.

The evolution of the ground-state populations is completely determined by the three parameters ξ_{pol} , γ_p , and γ_1 . If we choose $1/\gamma_1$ as the time unit, the time-dependent solutions of Eqs. (2.11) and (2.12) depend only on the dimensionless parameters γ_p/γ_1 and ξ_{pol} . We have calculated the evolution of the populations $p_{F,M}$ as follows. The system of differential equations can be rewritten in the form

$$\frac{d\vec{P}}{dt} = \mathcal{M}\vec{P} - \vec{P}_0, \quad (2.16)$$

where the components of \vec{P} (\vec{P}_0) are the populations (equilibrium populations) in the ground states $|F,M\rangle$ and \mathcal{M} is the pumping-relaxation matrix. The time dependence of the 16 ground-state populations $p_{F,M}$ is then calculated as the numerical solution of the system of Eqs. (2.11) and (2.12). With the normalization $\sum_{F,M} p_{F,M} = 1$, the polarizations of the hyperfine levels,

$$F_4 := \langle F_z \rangle_4 = \sum_M p_{4,M} M, \quad (2.17)$$

$$F_3 := \langle F_z \rangle_3 = \sum_M p_{3,M} M,$$

can be determined for the two extreme cases of pure repopulation and pure depopulation pumping. The results are shown in Fig. 2. At the beginning of the optical pumping process the hyperfine polarization F_3 decreases in both cases. In contrast to depopulation pumping, where F_3 remains negative, the polarization F_3 changes sign and becomes positive in the case of repopulation pumping.

B. Laser-induced fluorescence detection of spin polarization

In the experiments described below the atomic signal is recorded by detecting the resonance fluorescence emitted by

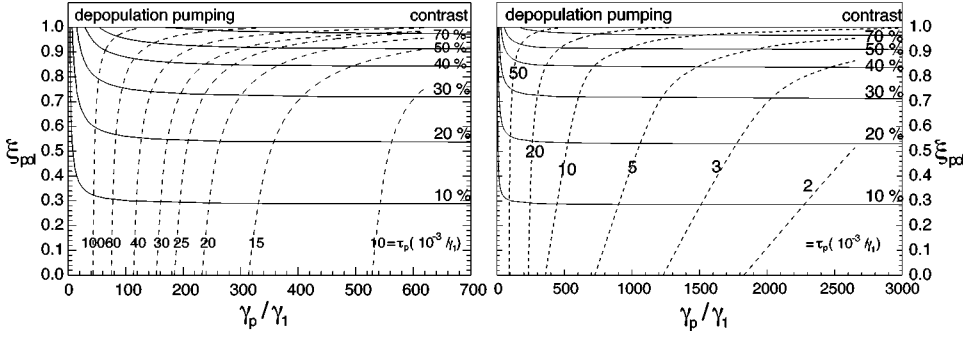


FIG. 4. Lines of constant contrast K (solid line) and lines of constant pump time τ_p in units of $10^{-3}/\gamma_1$ (dashed line) for depopulation pumping.

the Cs atoms upon illumination with circularly polarized light. As shown in the Appendix, the fluorescence rate from the spin polarized sample is given by

$$\mathcal{F} = \mathcal{F}_{\text{unpol}} \left(1 - \frac{1}{4} (F_4 - F_3) \right), \quad (2.18)$$

$$\mathcal{F} = \mathcal{F}_{\text{unpol}} (1 - 2\langle J_z \rangle), \quad (2.19)$$

where $\mathcal{F}_{\text{unpol}}$ is the rate of fluorescence emitted by the unpolarized sample ($\langle J_z \rangle = 0$). The fact that \mathcal{F} is independent of F and/or I reflects the property that the hyperfine levels are not resolved in the optical spectrum. As an example, in Fig. 3 we show the calculated time dependence of the normalized fluorescence signal after turning on the pumping light at $t=0$.

The relaxation rate γ_1 is the only parameter from the parameter set $\{\xi_{\text{pol}}, \gamma_p/\gamma_1\}$ which can be determined accurately in experiment. The pumping rate γ_p and the degree of circular polarization ξ_{pol} inside the cryostat are difficult to access experimentally. In the following we show how these parameters can be determined from the characteristic features of the experimental fluorescence decay curves. We introduce two parameters, which are readily determined in experiment, viz. the contrast K of the fluorescence and the pumping time τ_p . K is defined as the relative change of the fluorescence signal due to optical pumping:

$$K = \frac{\mathcal{F}(t=0) - \mathcal{F}(\infty)}{\mathcal{F}(t=0)} = 2\langle J_z \rangle. \quad (2.20)$$

As the decay of fluorescence in multilevel systems is in general nonexponential, we define the time constant τ_p as the time interval needed to build up 50% of the maximum achievable contrast K for a given set of parameters:

$$\mathcal{F}(\tau_p) - \mathcal{F}(0) = \frac{1}{2} (\mathcal{F}(\infty) - \mathcal{F}(0)). \quad (2.21)$$

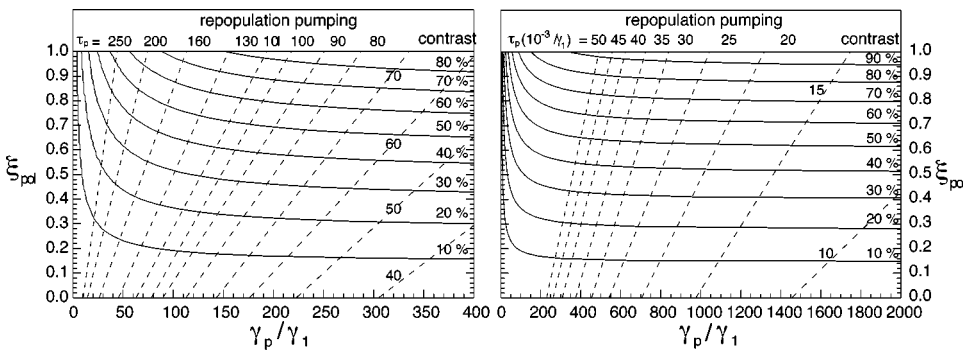


FIG. 5. Lines of constant contrast K (solid line) and lines of constant pump time τ_p in units of $10^{-3}/\gamma_1$ (dashed line) for repopulation pumping.

Note that the pumping time defined in this way is not to be confused with the inverse of the pump rate γ_p used as a parameter in the calculations. The pumping time constant τ_p and the contrast K of the fluorescence signal do not only depend on γ_p and ξ_{pol} , but also on the nature of the optical pumping process (repopulation or depopulation pumping in the extreme cases). From the numerical solutions of Eqs. (2.11) and (2.12), we have therefore determined the combinations of parameters ξ_{pol} and γ_p/γ_1 , which lead to a given time constant τ_p and to a given contrast K . In Figs. 4 and 5, these results are plotted as ‘‘isocontrast’’ and ‘‘isopumping time’’ curves for the cases of pure repopulation and pure depopulation pumping. A comparison of the measured parameters τ_p and K with these diagrams will allow us to determine ξ_{pol} and γ_p/γ_1 . These results, together with the known relaxation rate γ_1 , then yield the whole parameter set needed for the description of the evolution of the electronic ground-state polarization under optical pumping.

C. Optically detected magnetic resonance (ODMR)

The spin-polarized sample is characterized by a large population of the dark state $|F=4, M=4\rangle$. When the Zeeman degeneracy of the ground-state levels is lifted by a longitudinal magnetic field, resonant radio-frequency radiation can induce transitions between neighboring magnetic sublevels, resulting in a resonant sample depolarization and a corresponding increase of the optical scattering rate (fluorescence level). The basic properties and applications of this technique were reviewed, e.g., by Suter and Mlynek [16]. In a low magnetic field the Zeeman effect is linear, and all magnetic transition frequencies in a given hyperfine state F are degenerate. In larger fields the energies of the spin states $|F_{\pm}, M\rangle$ of the Cs ground state ($|F_{\pm} = I \pm \frac{1}{2}; M; J = S = \frac{1}{2}; I = 7/2\rangle$) are given by the Breit-Rabi formula [17]

$$\frac{\nu(F_{\pm}, M)}{\nu_{\text{hfs}}} = -\frac{1}{16} - M\epsilon x \pm \frac{1}{2} \sqrt{1 + \frac{1}{2}M(1+\epsilon)x + (1+\epsilon)^2 x^2}, \quad (2.22)$$

with

$$x = \frac{g_J \mu_B}{h \nu_{\text{hfs}}} B, \quad (2.23)$$

$$\epsilon = \frac{g_N \mu_N}{g_J \mu_B},$$

where g_J and g_N are the electronic and nuclear g factors, and μ_B and μ_N are the Bohr and nuclear magnetons, respectively. Expanding Eq. (2.22) up to first order in ϵ and to second order in x , the transition frequencies $\Delta \nu_{F_{\pm}, M}$ between neighboring spin states $|F, M+1\rangle$ and $|F, M\rangle$ are given by

$$\Delta \nu_{F_{\pm}, M} = \frac{\nu(F_{\pm}, M+1) - \nu(F_{\pm}, M)}{\nu_{\text{hfs}}} = \frac{1}{8} x \mp \frac{8 \mp 1}{8} \epsilon x - \frac{1}{64} (2M+1) x^2. \quad (2.24)$$

The first and second terms are linear contributions from the electronic and nuclear magnetic moments; the third term is the quadratic Breit-Rabi correction. As seen in Fig. 2, for the case of *repopulation pumping* the populations in both the $F=4$ and 3 hyperfine levels will be transferred into sublevels with the *same sign* of the magnetic quantum numbers M ($F_4/F_3 > 0$), whereas for *depopulation pumping* the steady-state hyperfine polarizations F_4 and F_3 will have opposite signs ($F_4/F_3 < 0$). The last term in Eq. (2.24) is proportional to $2M+1$, and the curvature of the quadratic field dependence of the transition frequency $\Delta \nu$ can therefore be used to discriminate depopulation from repopulation pumping.

III. EXPERIMENTAL SETUP

The experiments were performed in a cubic pressure cell immersed in a helium bath cryostat (Fig. 6). Temperatures down to 1.5 K could be reached by pumping on the helium bath. The pressure cell (inner volume $\approx 200 \text{ cm}^3$) has five quartz windows flanged onto its cubic body using soft-annealed copper sealing rings. The temperature inside the cell was measured with a germanium resistor, and all electrical feedthroughs were sealed with Stycast 2850 epoxy. The cell is connected via a capillary to an external reservoir of pressurized helium gas. By controlling the temperature and pressure in the cell helium crystals could be grown with either a bcc or hcp structure [18]. Cs atoms were implanted into the helium solid by laser ablation [19] with a beam from a pulsed, frequency-doubled Nd:YAG (yttrium aluminum garnet) laser (typically 20 mJ at a 1-Hz repetition rate). The laser beam was focused onto an alkali-metal target contained in a glass tube using a height-adjustable lens above the pres-

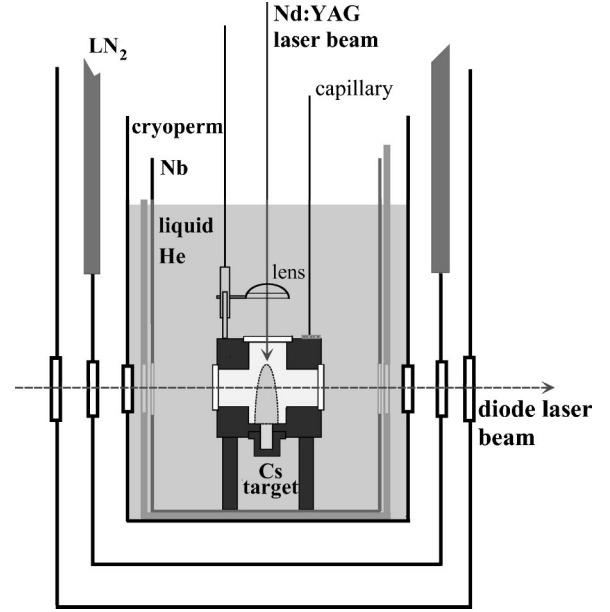


FIG. 6. Cross section of the bath cryostat and the He pressure cell.

sure cell. After the implantation process the lens was raised to allow the focussing of further Nd:YAG laser pulses with lower intensity into the center of the alkali-doped part of the He crystal. We observed a slow temporal decrease of the atomic fluorescence signal which we attribute to the combined action of diffusion and recombination of atoms with clusters and neighbouring atoms. The low-energy Nd:YAG pulses serve to dissociate these clusters and to stabilize the average atomic concentration. An almost constant number of atoms could be maintained during the experiments by applying these dissociation pulses at a constant repetition rate. A 2-mm-thick μ -metal (cryoperm) shield and a superconducting Nb shield surrounding the cell inside the helium bath reduce stray magnetic fields. Three orthogonal pairs of Helmholtz coils mounted around the pressure cell were used to apply homogeneous static magnetic fields. Inside of the cell three additional sets of Helmholtz coils allowed to irradiate the sample with radio-frequency fields. The Cs atoms were excited with a circularly polarized beam from a temperature stabilized monomode diode laser operating at 850 nm. Fluorescence from the sample was collected by a system of lenses and detected by a cooled RCA-C31034 photomultiplier. An interference filter ($T=78\%$ at 887 nm, and a full width at half maximum of 9 nm) suppressed scattered laser light by four orders of magnitude.

IV. EXPERIMENTS

We have performed experiments on Cs atoms in the isotropic bcc phase and in the anisotropic hcp phase of solid ^4He with the aim of understanding the dynamics and the mechanisms governing the optical pumping process in these samples.

A. Optical pumping process in the bcc phase

In a first series of experiments we have studied magnetic-resonance signals in small ($B_0 \leq 500 \text{ mG}$) magnetic fields.

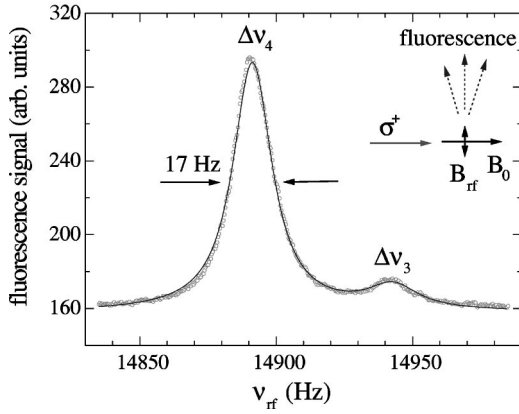


FIG. 7. ODMR spectrum in the ground state of Cs in bcc ^4He in a magnetic field of 43 mG. The splitting of the lines is a consequence of the nuclear magnetic moment and the quadratic Zeeman effect.

The sample—exposed to a constant magnetic field—was irradiated with circularly polarized light, and the fluorescence signal was recorded while the frequency of a linearly polarized radio-frequency field was swept across the resonances. A typical spectrum (integration time of 0.5 s per data point) is shown in Fig. 7. The two resonances ($\Delta\nu_4$ and $\Delta\nu_3$) in Fig. 7 correspond to rf-induced depolarizing transitions in the $F=4$ and 3 states, respectively. The line splitting is a consequence of the nuclear magnetic moment and of the quadratic Zeeman effect of the electronic magnetic moment [Eq. (2.24)]. We have recorded such doublets with both σ_+ and σ_- excitation for ten values of B_0 in the range 0–500 mG. The line centers were obtained by fitting the experimental data with Lorentzians and a constant background. The small widths of the magnetic resonance lines and their large signal-to-noise ratio allow the determination of the line centers with sub-Hz precision [8]. In order to observe both hyperfine states the laser intensity was adjusted to be low enough to guarantee that both the $F=3$ and 4 states were populated. As a consequence the sublevel populations in these states are distributed over several M values, and the factor $2M+1$ in the expression for the quadratic Zeeman effect has to be replaced by $2\langle M \rangle_F + 1 = 2\langle F_z \rangle_F + 1$. Equation (2.24) can therefore not be applied directly to analyze the resonance frequencies. When the helicity of the pumping light is reversed under otherwise identical conditions, the sign of this term is reversed. The quadratic Zeeman term can be extracted by subtracting (for each value of B_0) the resonance frequencies obtained with σ_+ and σ_- excitation. The magnetic-field dependences of these difference frequencies $\Delta\nu_4(\sigma_-) - \Delta\nu_4(\sigma_+)$ and $\Delta\nu_3(\sigma_-) - \Delta\nu_3(\sigma_+)$ are shown in Fig. 8. The anticipated quadratic field dependence is confirmed by the fitted parabolas (solid lines). The curvatures for both hyperfine states are of equal sign, thus giving evidence that *repopulation pumping* (cf. Fig. 1) is the main mechanism governing the optical pumping process of Cs atoms trapped in the bcc phase of ^4He .

As we shall see below, optical pumping in the hcp phase is in strong competition with fast spin-relaxation processes, yielding correspondingly larger magnetic resonance linewidths. The above technique cannot be applied to study the pumping mechanism in that phase, as substantially larger

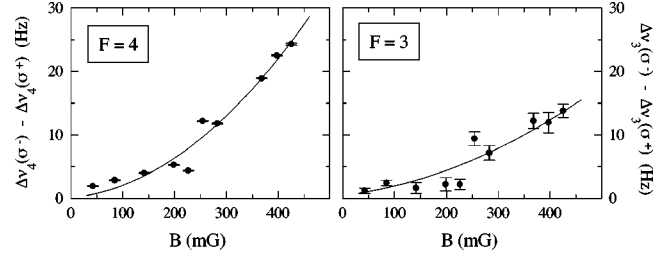


FIG. 8. Difference of the Larmor frequencies (cf. Fig. 7) in $F=4$ and 3 when excited with σ_+ and σ_- light. The observed field dependence reflects the quadratic term of the Breit-Rabi formula, and allows one to distinguish repopulation from depopulation pumping.

magnetic fields will be needed to split the two lines. As shown in Sec. II, repopulation pumping can also be distinguished from depopulation pumping from the parameters describing the time dependence of the fluorescence signal when the system evolves from an unpolarized state to a polarized state. In order to check the usefulness of this alternative approach, we have performed a second experiment in the bcc phase. In this investigation F -state-selective radio-frequency π pulses were applied to flip the polarization in the $F=4$ or 3 states selectively, and the optical pumping mechanism is inferred by comparing experimental fluorescence decay signals with calculated temporal evolutions. An acousto-optical modulator was used for switching the circularly polarized optical pumping light intensity. A longitudinal constant magnetic field of 500 mG was applied along the propagation direction of the laser light. The longitudinal pumping process is detected by monitoring the time dependence of the laser-induced fluorescence. A typical signal is shown in Fig. 9. After switching on the laser at $t=0$, the increase of the spin polarization manifests itself by a decrease of the fluorescence signal [see Eq. (2.18)]. The signal level at $\mathcal{F}(t=0)$ is a measure of the unpolarized fluorescence rate $\mathcal{F}_{\text{unpol}}$. After 200 ms the system is fully polarized. The light is then turned off for 5 ms, and a radio-frequency π pulse of duration $\tau_\pi = 5$ ms is applied in order to rotate the polarization $\langle F_z \rangle$ in the $F=4$ or 3 state *selectively* by 180° . The spin-flip occurs in the dark, and guarantees that the polarization is not af-

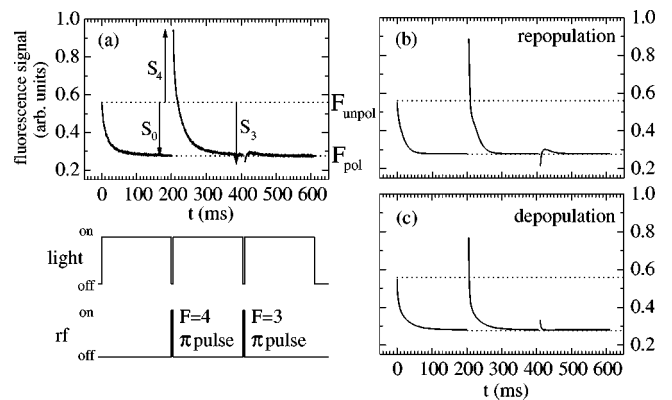


FIG. 9. Experimental (a) and calculated [(b) and (c)] evolution of fluorescence signals after application of a radio-frequency π pulse for $F=3$ (at $t=200$ ms) and for $F=4$ (at $t=405$ ms). The theoretical curves are shown for the case of repopulation (b) and depopulation (c) pumping.

ected by optical pumping during the magnetic-resonance transition. Due to the second term in Eq. (2.24), the Larmor frequency in $|F=3\rangle$ is about 585 Hz higher than in $|F=4\rangle$ at the given magnetic field $B=500$ mG. As the spectral width of the pulse $(2\pi\tau_\pi)^{-1}=32$ Hz is much smaller than the difference of these Larmor frequencies, the polarizations in the hyperfine ground states can be flipped selectively by applying the appropriate radio frequency. After the π pulses the pumping light is switched on again at $t=205$ and 410 ms, and the fluorescence signal is allowed to evolve towards its steady-state value \mathcal{F}_{pol} .

For the analysis we introduce the following notation. S_0 is the asymptotic fluorescence level of the polarized sample, and S_3 and S_4 are the fluorescence levels right after the π pulses:

$$S_0 = \mathcal{F}_{\text{unpol}} - \mathcal{F}_{\text{pol}} = \frac{F_4 - F_3}{4},$$

$$S_4 = \frac{-F_4 - F_3}{4} \quad (\text{after the } \pi \text{ pulse in } F=4), \quad (4.1)$$

$$S_3 = \frac{F_4 + F_3}{4} \quad (\text{after the } \pi \text{ pulse in } F=3).$$

The theoretical calculation predicts that the expectation values $F_4 = \langle F_z \rangle_{F=4}$ and $F_3 = \langle F_z \rangle_{F=3}$ are of equal sign for repopulation pumping, whereas for depopulation pumping they have opposite signs. These signs can be inferred by comparing S_0 with S_3 and S_4 respectively. From Eq. (4.1) one sees that $\text{sgn}(F_4) = \text{sgn}(F_3)$ when $|S_3| > |S_0|$, or, equivalently, when $|S_4| > |S_0|$. The experimental data in Fig. 9 show that both $|S_4| > |S_0|$ and $|S_3| > |S_0|$. The hyperfine polarizations F_4 and F_3 thus have identical signs. This gives another independent proof that in the isotropic bcc phase of solid ^4He the electronic ground state of the trapped Cs atoms is polarized mainly by optical *repopulation pumping*.

Finally we show how the model can be applied to calculate the complete time evolution of the fluorescence signal. The experiments were performed in the bcc phase, where the longitudinal relaxation rate γ_1 is 1 s^{-1} (Fig. 10). From the experimental data in the range $0 < t < 200$ ms (Fig. 9), we obtain a pumping time τ_p of 10 ms and an experimental contrast K_{expt} of 49%. In order to infer the contrast due to spin polarization only we have to consider that the detected signal is a superposition of atomic resonance fluorescence and a constant background signal C which originates from light scattered by molecules and clusters in the sample. In an auxiliary experiment the intensity of scattered light was determined to be 40% of the unpolarized fluorescence level $\mathcal{F}_{\text{unpol}}$. Taking this additional signal into account the contrast K due to spin polarization only is given by

$$K = 1 - \frac{\mathcal{F}_{\text{pol}} + C}{\mathcal{F}_{\text{unpol}} + C} = 69\%, \quad (4.2)$$

where $C = 0.4\mathcal{F}_{\text{unpol}}$. Using the calculated isocontrast and isopumping time curves of Figs. 4 and 5 together with the

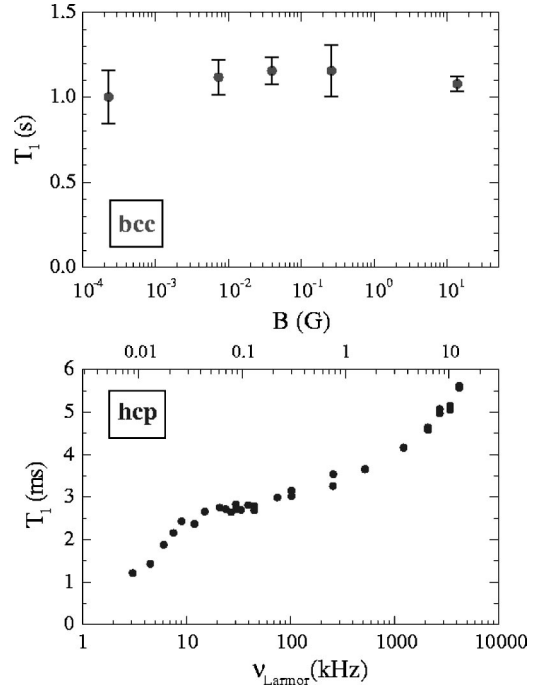


FIG. 10. Magnetic-field dependence of the longitudinal relaxation times T_1 of $\langle J_z \rangle$ of Cs in bcc and hcp ^4He . The gyromagnetic ratio of the $6S_{1/2}$ hyperfine states is 350 kHz/G.

measured parameters $\gamma_1 = 1 \text{ s}^{-1}$, $\tau_p = 10$ ms, and $K = 69\%$, we infer a parameter γ_p/γ_1 of 2450 and a degree of circular polarization ξ_{pol} of 79% in case of repopulation pumping, and $\gamma_p/\gamma_1 = 2500$ and $\xi_{\text{pol}} = 97\%$ for depopulation pumping. Using these parameters the time evolution of the fluorescence signal is calculated for repopulation and depopulation pumping (Fig. 9). The F -selective experimental π pulses are simulated by interchanging $p_{4,M} \leftrightarrow p_{4,-M}$ at $t = 205$ ms and $p_{3,M} \leftrightarrow p_{3,-M}$ at $t = 410$ ms. After the respective rotations of the population vectors the calculation of the time dependence of the fluorescence signal is resumed using the same procedure as before. The good agreement of the experimental fluorescence signals with the calculated signals then gives the final proof that repopulation is the main pumping mechanism, as only for this process the fluorescence signal will change sign with respect to the unpolarized level $\mathcal{F}_{\text{unpol}}$. Knowing the pumping mechanism and the experimental parameters ξ_{pol} , γ_p/γ_1 , and τ_p , the complete evolution of the fluorescence signal can then be simulated, and agrees well with the experimental findings (Fig. 9).

B. Optical pumping process in the hcp phase

Since the first optical pumping experiments on Cs in solid He matrices [7] it was known that optical pumping in hcp crystals is much less efficient than in bcc crystals. This is best evidenced by the longitudinal spin relaxation times T_1 in the two phases. T_1 was measured as a function of the longitudinal magnetic field B_0 using the method of “relaxation in the dark” [7,20]. In Fig. 10 we compare the results obtained in hcp matrices to our earlier results obtained in bcc matrices. In the hcp phase the spin relaxation time T_1 is 2–3 orders of magnitude smaller than in the bcc phase while in the bcc phase T_1 is independent of the strength of the hold-

ing field,² it shows a pronounced magnetic-field dependence in the hcp phase with a cusp-shaped structure around $\nu_L \approx 10$ kHz. We believe that the origin of the lower pumping efficiency observed in the hcp phase is a slight (nonspherical) static deformation of the shape of the local trapping sites (atomic bubbles). Recently we explained the unexpected redshift of the hyperfine transitions in the hcp phase in terms of a small (5%) quadrupolar deformation [13] of the atomic bubbles in that phase. The observations made here can be explained qualitatively as follows: In small magnetic fields (Larmor frequency $\ll 10$ kHz) the magnetic moments of the Cs atoms couple to the randomly oriented rotational symmetry axes of the deformed bubbles. As a consequence the sample is strongly depolarized. In larger fields the Zeeman interaction decouples the magnetic moments from the spin-bubble axis interaction, which leads to a B -dependent lengthening of the relaxation times. This phenomenon has a close analogy with the well-known Zeeman decoupling from hyperfine or spin-orbit interactions (Breit-Rabi problem).

The saturation behavior (plateau in the range 10–100 kHz) allows us to estimate the strength of the spin-bubble axis coupling to be on the order of 10 kHz. The deformed bubbles lift the Zeeman degeneracy in the ground state of the Cs atoms in the hcp phases, as we have shown experimentally by the observation of zero-field magnetic-resonance spectra [13]. It is interesting to note here that the most pronounced structure in these zero-field spectra also occurs at approximately 10 kHz. The origin of the observed increase of T_1 above 100 kHz is not clear at present. It may be related to a Zeeman decoupling from F -changing interactions with the deformed bubbles for which the decoupling field strength is on the order of 2–4 kG. Future experiments in larger fields should shine more light on this hypothesis.

Due to the small relaxation times in the hcp phase which lead to magnetic-resonance linewidths of several kHz, the experiments described above for the bcc phase cannot be performed in the hcp phase. Our current setup allows us to apply fields only up to 10 G (a Larmor frequency of 3.5 MHz), for which the $F=3$ and 4 components cannot be resolved, so that F -state-selective π pulses cannot be applied to the sample.

In the following we show how the mechanism of the optical pumping process in the hcp phase can nevertheless be inferred from contrast measurements. For this analysis we start from a set of fluorescence time evolution curves recorded in different longitudinal magnetic fields B when the sample is optically pumped with a fixed laser intensity (pump rate) (Fig. 11). The contrasts are inferred from the asymptotic fluorescence levels and their magnetic field dependence is shown in Fig. 12. For the data recorded at $B = 12$ G, from Figs. 10, 11 and 12 we infer a relaxation rate γ_1 of 200 s^{-1} , a pumping time τ_p of 1 ms (i.e., $\tau_p = 200 \cdot 10^{-3} / \gamma_1$), and a contrast K of 36%. Using these parameters we obtain values $\xi_{\text{pol}} = 70\%$ and $\gamma_p / \gamma_1 = 50$ from the calculated isocontrast and isopump-time diagrams for repopulation pumping (Fig. 5). If the optical pumping would

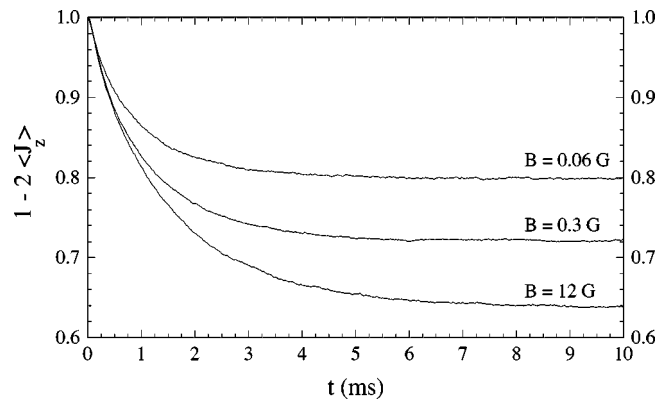


FIG. 11. Measured time evolution of the (normalized) fluorescence signals in hcp ^4He for different values of the magnetic field B . The asymptotic values yield the contrast K .

proceed via depopulation pumping (Fig. 4), the observed contrast could not be achieved even with a degree of circular polarization ξ_{pol} of 100%. This is a clear evidence that optical pumping of Cs in hcp ^4He is also dominated by repopulation pumping, i.e., that both in bcc and in hcp He crystals the spin polarization in the excited state is not noticeably destroyed by the interaction with the helium matrix.

V. DISCUSSION AND CONCLUSION

We have carried out a detailed study of the mechanism governing the optical pumping of Cs atoms implanted in helium crystals. We find that both in the isotropic bcc phase and in the uniaxial hcp phase, optical pumping is dominated by repopulation, i.e., Kastler-type pumping. This result is surprising at first sight. It is well known that in Cs vapor the addition of He buffer gas leads to a rapid spin depolarization in the excited state already for moderate buffer gas pressures. In solid He the surrounding He atoms collide with the Cs atom at the rate of helium lattice vibrations (the Debye frequency is 4×10^{12} Hz). The fact that the polarization of the $P_{1/2}$ state survives this high collision rate lies in the short duration of the collision which is comparable to the inverse collision rate. A single collision can be viewed as a momentary deformation of the Cs bubble. As the interaction of the spin with deformed bubbles is very weak (10-kHz coupling strength with a 5% quadrupolar bubble deformation) the

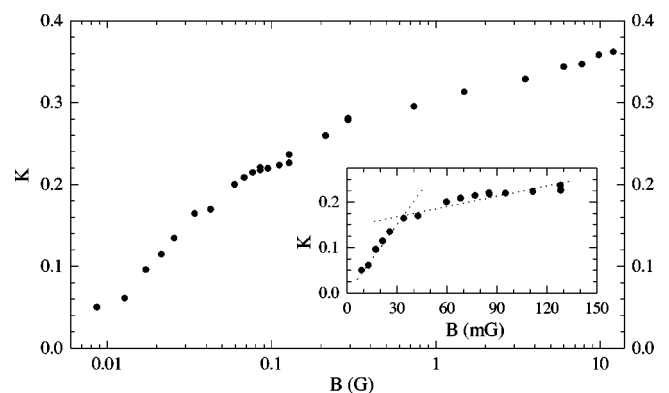


FIG. 12. Magnetic-field dependence of the fluorescence contrast K in hcp ^4He ($T = 1.5$ K, $p = 27$ bar).

²The physical mechanism that determines T_1 in the bcc phase is not yet understood. This is likely to be due to the depolarizing effect of quadrupolar oscillations of the bubble shape.

spins have no time to undergo a significant dephasing during the collision time. Some caution should nevertheless be expressed regarding the above results. In the model calculations presented above we assumed the spin relaxation in the ground state to be isotropic, i.e., independent of M . While this assumption certainly holds for bcc matrices it is certainly no longer valid in hcp matrices, where we believe that randomly oriented bubble deformations are responsible for the spin depolarization. In order to incorporate these anisotropic relaxation processes into model calculations, a better understanding of the coupling mechanism of the spins to the axis of deformed bubbles is required. Work toward this goal is currently in progress.

Another important consequence of repopulation pumping is the fact that the resonance fluorescence is polarized. This opens the possibility to measure the product $g_J(6P_{1/2})\tau(6P_{1/2})$ of the $6P_{1/2}$ state using the Hanle effect and to determine, in combination with a direct measurement of the $6P_{1/2}$ lifetime $\tau(6P_{1/2})$, the Landé g factor of this state. We are currently preparing such experiments.

Recently we have detected isotopes 85 and 87 of Rb in solid helium using an absorption technique. The magnetic resonance spectra give strong evidence that for these atoms depopulation, i.e., Dehmelt-type pumping is the main mechanism governing the buildup of spin polarization. A detailed account of these experiments and their interpretation will be given elsewhere.

ACKNOWLEDGMENTS

This work was supported by research Grant No. WE2202/4-1 of the Deutsche Forschungsgemeinschaft, and by INTAS (Grant No. 96-0334).

APPENDIX

The goal of this appendix is to express the fluorescence rate in terms of physical observables. We start by noting that under linear, i.e., nonsaturating excitation, the fluorescence rate is proportional to the optical absorption coefficient κ . Due to the large homogeneous broadening of the optical line, saturation phenomena can be neglected. For the same reason the hyperfine structure in both the excited and ground states is not resolved in the optical spectra. The total absorption coefficient κ_{tot} can thus to be expressed as the weighted sum of the transition probabilities of all electric dipole allowed transitions from the ground-state sublevels $|F, M\rangle \equiv |6^2S_{1/2}, F, M\rangle$ to the excited-state sublevels $|f, m\rangle \equiv |6^2P_{1/2}, f, m\rangle$, i.e.,

$$\kappa_{\text{tot}} = \sum_{f=3}^4 \sum_{m=-f}^f \sum_{F=3}^4 \sum_{M=-F}^F P_{FM} \kappa_{F, M \rightarrow f, m} \quad (\text{A1})$$

The weighting factors p_{FM} are the populations of the levels $|F, M\rangle$. The individual transition probabilities are proportional to the squares of the relevant matrix elements, which are readily expressed in terms of $3j$ and $6j$ symbols [21]:

$$\begin{aligned} \kappa_{F, M \rightarrow f, m} &\propto |\langle f, m | x_q | F, M \rangle|^2 = (2F+1)(2f+1) \\ &\times \left(\begin{array}{ccc} f & 1 & F \\ -m & q & M \end{array} \right)^2 \left\{ \begin{array}{ccc} \frac{1}{2} & f & \frac{7}{2} \\ F & \frac{1}{2} & 1 \end{array} \right\}^2 \\ &\times |\langle 6^2P_{1/2} || r || 6^2S_{1/2} \rangle|^2. \end{aligned}$$

Under excitation with σ_+ circularly polarized light ($q = +1$), the relative transition probabilities are [21]

$$\begin{aligned} \kappa_{3, M \rightarrow 3, M+1} &\propto (3-M)(4+M), \\ \kappa_{3, M \rightarrow 4, M+1} &\propto (4+M)(5+M), \\ \kappa_{4, M \rightarrow 3, M+1} &\propto (3-M)(4-M), \\ \kappa_{4, M \rightarrow 4, M+1} &\propto (4-M)(5+M), \end{aligned}$$

and the total absorption coefficient can be evaluated algebraically to yield

$$\kappa_{\text{tot}} \propto 4p_{\text{tot}} + \sum_M M(p_{3M} - p_{4M}), \quad (\text{A2})$$

where $p_{\text{tot}} = \sum_{F, M} P_{FM}$ is the total population of the ground state. If the sample is unpolarized the populations are given by their statistical weights, and we refer to the corresponding value of the absorption coefficient as the unpolarized absorption coefficient κ_{unpol} . This determines the proportionality coefficient in Eq. (A2), which may thus be rewritten as

$$\kappa_{\text{tot}} = \kappa_{\text{unpol}} \left[1 - \frac{F_4 - F_3}{4} \right], \quad (\text{A3})$$

where F_3 and F_4 are the expectation values of F_z in the hyperfine levels $F=3$ and $F=4$ respectively, i.e.,

$$\langle F_z \rangle_F = \frac{1}{p_{\text{tot}}} \sum_M \langle F, M | F_z | F, M \rangle p_{F, M}.$$

Using well-known properties [21] of the matrix elements of J_z and F_z , one may show that Eq. (A3) is equivalent to

$$\kappa_{\text{tot}} = \kappa_{\text{unpol}} [1 - 2\langle J_z \rangle]. \quad (\text{A4})$$

This result does not depend on the hyperfine quantum numbers F and f , which makes sense if one considers that the hyperfine structure is not resolved in the absorption and fluorescence spectra.

- [1] H. Coufal, E. Luescher, H. Micklitz, and R. E. Norberg, *Rare Gas Solids*, Springer Tracts in Modern Physics, Vol. 103, (Springer, Berlin, 1984).
 [2] S. I. Kanorsky, M. Arndt, R. Dziewior, A. Weis, and T. W. Hänsch, *Phys. Rev. B* **49**, 3645 (1994).

- [3] M. Arndt, S. I. Kanorsky, A. Weis, and T. W. Hänsch, *Phys. Lett. A* **174**, 298 (1993).
 [4] A. Fujisaki, K. Sano, T. Kinoshita, Y. Takahashi, and T. Yabuzaki, *Phys. Rev. Lett.* **71**, 1039 (1993).
 [5] T. Kinoshita, Y. Takahashi, and T. Yabuzaki, *Phys. Rev. B* **49**,

- 3648 (1994).
- [6] Y. Takahashi, K. Fukuda, T. Kinoshita, and T. Yabuzaki, *Z. Phys. B* **98**, 391 (1995).
- [7] M. Arndt, S. I. Kanorsky, A. Weis, and T. W. Hänsch, *Phys. Rev. Lett.* **74**, 1359 (1995).
- [8] S. I. Kanorsky, S. Lang, S. Lücke, S. B. Ross, T. W. Hänsch, and A. Weis, *Phys. Rev. A* **54**, R1010 (1996).
- [9] A. Weis, S. Kanorsky, S. Lang, and T. W. Hänsch, in *Atomic Physics Methods in Modern Research*, edited by K. Jungmann, J. Kowalski, I. Reinhard, and F. Träger, *Lecture Notes in Physics*, Vol. 499 (Springer, Berlin, 1997), pp. 57–75.
- [10] S. I. Kanorsky and A. Weis, *Adv. At., Mol., Opt. Phys.* **38**, 87 (1998).
- [11] S. I. Kanorsky and A. Weis, in *Quantum Optics of Confined Systems*, edited by M. Ducloy and D. Bloch, *Applied Sciences*, Vol. 314 (Kluwer, Dordrecht, 1996), pp. 367–393.
- [12] B. Tabbert, H. Günther, and G. zu Putlitz, *J. Low Temp. Phys.* **109**, 653 (1997).
- [13] S. Kanorsky, S. Lang, T. Eichler, K. Winkler, and A. Weis, *Phys. Rev. Lett.* **81**, 401 (1998).
- [14] J. Brossel and A. Kastler, *C. R. Hebd. Seances Acad. Sci.* **229**, 1213 (1949).
- [15] W. Happer, *Rev. Mod. Phys.* **44**, 169 (1972).
- [16] D. Suter and J. Mlynek, *Adv. Magn. Opt. Reson.* **16**, 1 (1991).
- [17] G. Breit and I. I. Rabi, *Phys. Rev.* **38**, 2082 (1931).
- [18] S. Lang, M. Arndt, T. W. Hänsch, S. I. Kanorsky, S. Lücke, S. Ross, and A. Weis, *Low Temp. Phys.* **22**, 129 (1996).
- [19] M. Arndt, S. I. Kanorsky, A. Weis, and T. W. Hänsch, *Z. Phys. B* **98**, 377 (1995).
- [20] A. Weis, S. Lang, S. I. Kanorski, M. Arndt, S. B. Ross, and T. W. Hänsch, *Proceedings of the 12th International Conference on Laser Spectroscopy*, edited by M. Inguscio, M. Allegrini, and A. Sasso (World Scientific, London, 1996).
- [21] I. I. Sobelman, *Atomic Spectra and Radiative Transitions*, *Springer Series in Chemical Physics* (Springer, Berlin, 1979).